ATLAS NOTE

ATLAS-CONF-2012-155

November 12, 2012

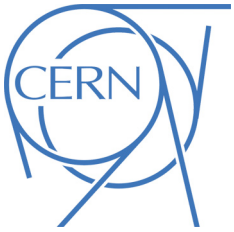

Measurement of the jet multiplicity in top–anti-top final states produced in 7 TeV proton–proton collisions with the ATLAS detector

The ATLAS Collaboration

Abstract

The jet multiplicity is measured for a single-lepton top anti-top ($t\bar{t}$) event selection, in proton–proton collisions at a centre-of-mass energy of 7 TeV, for jet transverse momentum thresholds of 25, 40, 60, and 80 GeV. Results are shown for an integrated luminosity of 4.7 fb^{-1}. After background subtraction, the reconstructed spectra are fully corrected for all detector effects within a kinematic range closely matched to the experimental acceptance. The measurements are compared to several Monte Carlo models, which include fixed order matrix element calculations and experimentally motivated variations of initial and final state radiation. The MC@NLO generator is found to consistently predict fewer jets than the measured spectra. Constraints are set on the modelling of additional radiation with the ALPGEN generator interfaced with the PYTHIA parton shower, which are consistent with previous measurements.

ATLAS-CONF-2012-155
12 November 2012

1 Introduction

The inclusive top anti-top ($t\bar{t}$) production cross-section has been measured in proton–proton (pp) collisions at a centre-of-mass energy of 7 TeV by the ATLAS [1, 2] and CMS [3] collaborations. These measurements have been performed inclusively, using $t\bar{t}$ final states with an arbitrary number of additional jets.

In the Standard Model (SM), a top quark decays to a W boson and a b quark with a branching fraction close to unity. Experimentally, there are three $t\bar{t}$ signatures that correspond to different decay modes of the W bosons. In the case where one W boson decays leptonically, and the other one hadronically, the $t\bar{t}$ event is expected to contain one high-energy lepton, missing transverse energy associated with a neutrino, and at least four jets. These types of events will be referred to as the single-lepton channel. The presence of b-jets in $t\bar{t}$ events can be used to reduce the non-top SM backgrounds, which contain a small fraction of heavy flavour jets.

A measurement of $t\bar{t}$ production with additional jets and as a function of the jet transverse momentum (p_{T}) is useful to constrain models of initial and final state radiation (ISR/FSR) at the scale of the top quark mass, and also provides a test of perturbative QCD in the LHC energy regime. The ATLAS collaboration performed an initial measurement of the reconstructed jet multiplicity spectra from $t\bar{t}$ events, which was compared with Monte Carlo (MC) predictions [4]. This measurement was not corrected for detector effects and was dominated by systematic uncertainties. More recently, the fraction of events surviving a veto on additional jets in $t\bar{t}$ final states with two charged leptons has been measured as a function of the additional jet p_{T} threshold [5]. The measurement reported in Ref. [5] was used in this analysis to constrain the ISR/FSR uncertainties affecting $t\bar{t}$ MC samples.

This note presents the jet multiplicity measurements for four jet p_{T} thresholds (25, 40, 60, and 80 GeV) in the single-lepton channel, after correction for all detector effects through unfolding. The measurements are presented within a kinematic range corresponding to the acceptance of the reconstruction-level event selection.

2 The ATLAS detector

Due to the complexity of the final state in the selected events, the presented analysis relies on all main ATLAS detector subsystems. The ATLAS detector [6] at the Large Hadron Collider (LHC) [7] covers nearly the entire solid angle around the collision point. It consists of an inner tracking detector (ID), comprising a silicon pixel detector, a silicon microstrip detector (SCT), and a transition radiation tracker (TRT). The ID is surrounded by a superconducting solenoid providing a 2 T magnetic field. The ID is used for reconstruction of tracks and primary vertices and plays a crucial role in b-quark jet identification. It is surrounded by liquid-argon (LAr) electromagnetic (EM) sampling calorimeters with high granularity. An iron/scintillator tile calorimeter provides hadronic energy measurements in the central pseudorapidity[1] range ($|\eta| < 1.7$). The end-cap and forward regions are instrumented with LAr calorimeters for both electromagnetic and hadronic energy measurements up to $|\eta| = 4.9$. The information from the calorimeters and the inner tracking detector is used for electron identification and jet reconstruction. The calorimeter system is surrounded by a muon spectrometer (MS) incorporating a system of air-core superconducting toroid magnet assemblies.

The online event selection relies on a three-level trigger system. A hardware-based first level trigger reduces the event rate to less than 75 kHz. The detector readout is then available for two stages of

[1]The ATLAS reference system is a Cartesian right-handed co-ordinate system, with the nominal collision point at the origin. The anti-clockwise beam direction defines the positive z-axis, while the positive x-axis is defined as pointing from the collision point to the centre of the LHC ring and the positive y-axis points upwards. The azimuthal angle ϕ is measured around the beam axis, and the polar angle θ is measured with respect to the z-axis. The pseudorapidity is defined as $\eta = -\ln\tan(\theta/2)$.

software-based (higher-level) triggers. In the second level, partial object reconstruction is carried out to improve the selection and the associated rate. At the last level, the event filter, the full online event reconstruction is used and the rate is reduced to a level of approximately 300 Hz.

3 Event selection at the reconstruction level

3.1 Object reconstruction

Primary vertices were reconstructed from tracks within the ID. The selected primary vertex was required to have at least four tracks and to be consistent with the beam collision region in the $x-y$ plane. If more than one primary vertex candidate was found, then the vertex with the highest sum p_{T}^2 for associated tracks was chosen.

Electron candidates were identified [8] as energy deposits (clusters) in the electromagnetic calorimeters, with a matching reconstructed track in the inner detector. These electrons were selected within the pseudorapidity range $|\eta| < 2.47$, excluding the barrel/end-cap transition region of $1.37 < |\eta| < 1.52$. The associated energy cluster in the calorimeter was required to be isolated. The isolation requirement was formed by calculating the energy sum within a cone of radius $\Delta R = \sqrt{\Delta\eta^2 + \Delta\phi^2} = 0.2$ around the electron direction, after the exclusion of calorimeter cells associated with the electron cluster. Electrons were required to have an isolation below 10% of the electron energy. A similar isolation requirement was made on the track transverse momentum sum within a cone of radius $\Delta R = 0.3$ around the electron direction. To reduce the effects of additional primary vertices, the electron was required to have a longitudinal impact parameter with respect to the selected primary vertex of less than 2 mm. The reconstructed p_{T} of electrons used in the event selection was required to be greater than 25 GeV, but electrons with $p_{\mathrm{T}} > 15$ GeV were considered when removing jets that overlapped with electrons and when applying a veto on additional leptons.

Muon candidates were required to have a reconstructed track in the MS matched with a track reconstructed in the ID, a reconstructed p_{T} greater than 25 GeV and pseudorapidity $|\eta| < 2.5$. The selected muons were required to be isolated in the calorimeter and tracking volume. The calorimeter isolation was constructed from the energy sum within a cone of $\Delta R = 0.2$ around the direction of the muon and was required to be less than 4 GeV. The isolation within the ID was formed using a p_{T} sum of tracks within a cone of $\Delta R = 0.3$ around the direction of the muon and was required to be less than 2.5 GeV. To reduce the effects of additional primary vertices, the muon was required to have a longitudinal impact parameter with respect to the selected primary vertex of less than 2 mm. In the same manner as the electron selection, muons with p_{T} down to 15 GeV were used to veto additional leptons.

Topological clusters [9] were formed from calorimeter energy deposits. These clusters were used as input to the the anti-k_t jet algorithm [10] with a radius parameter of $R = 0.4$. Jets were required to have p_{T} greater than 25 GeV after energy calibration using the `EM+JES` scheme [11] and pseudorapidity $|\eta| < 2.5$. To avoid selecting jets from additional pp interactions, at least 75% of the sum of the p_{T} of tracks associated with a jet (JVF) was required to be from tracks compatible with the selected primary vertex. Jets with no associated tracks were also accepted.

During jet reconstruction no distinction was made between any identified electron and jet energy deposits. Therefore, the closest jet within a cone of $\Delta R = 0.2$ of any electron was removed. Muons which overlapped within $\Delta R = 0.4$ of any reconstructed jet of p_{T} greater than 25 GeV and JVF > 0.75 were removed.

An object-based scheme was used to calculate the missing transverse momentum, $E_{\mathrm{T}}^{\mathrm{miss}}$. Calorimeter cells were calibrated according to the object (electrons, photons, jets with $p_{\mathrm{T}} > 7$ GeV, and muons) with which they were associated. Cells not associated with an object were calibrated at the EM scale and included as a "Cell Out" term. The $E_{\mathrm{T}}^{\mathrm{miss}}$ was then calculated from the vector sum of electron, jet, muon

and Cell Out terms. This calibration scheme was similar to Ref. [12], and included the electron object definition used for this analysis.

A jet was identified as a b-jet using the MV1 algorithm [13], which combines several tagging algorithms. b-jets were selected with 70% efficiency for $p_{\mathrm{T}} > 15$ GeV in simulated $t\bar{t}$ events. The light jet rejection factor was 130.

3.2 Event selection

Data were selected from stable pp LHC running periods from the full 2011 ATLAS dataset. Data used in this measurement were collected by triggering on either a high-p_{T} electron, based on calorimeter energy deposits, shower shape and track quality constraints, or a high-p_{T} muon with a reconstructed track in the muon spectrometer matched with a track found in the inner detector. The p_{T} threshold for the muon trigger was 18 GeV and for the electron trigger was 20 GeV or 22 GeV, according to the data-taking period. Events were selected from periods during which all ATLAS sub-detectors were fully operational, which corresponded to an integrated luminosity of 4.7 ± 0.2 fb^{-1}.

The selected events were required to contain a reconstructed primary vertex. In the electron (muon) channel, signal candidate events were selected by requiring exactly one electron (muon) with $p_{\mathrm{T}} > 25$ GeV and events containing any additional leptons (electrons or muons) with $p_{\mathrm{T}} > 15$ GeV were vetoed. In both channels, the selected lepton was required to match the lepton reconstructed by the high-level trigger.

Events were required to have $E_{\mathrm{T}}^{\mathrm{miss}}$ greater than 30 GeV and a transverse W mass[2] $m_{\mathrm{T}}(W)$ greater than 35 GeV. Events were required to contain at least three selected jets with p_{T} greater than 25 GeV. At least one of these jets was required to be tagged as a b-jet.

Events were rejected which contained any jet with $p_{\mathrm{T}} > 20$ GeV that was identified as calorimeter noise or out-of-time activity with respect to the considered pp collision [14]. Events containing one or more selected electrons which included a reconstructed track associated with a muon were also rejected.

4 Monte Carlo simulation

MC simulated events were used to derive correction factors for the correction of the reconstructed spectra for all detector effects and to model some of the background contributions.

The nominal sample of top pair events was generated using the ALPGEN [15] v2.13 generator and CTEQ6L1 [16] PDF set. The sample was generated for $t\bar{t}$ with zero to four exclusive and five inclusive additional light partons. Parton showering and fragmentation was performed by HERWIG [17] v6.520. The MLM parton-jet matching scheme [15] was applied (`ETCLUS` 20 GeV, `RCLUS` 0.7, `ETACLUS` 6.0) to avoid double counting of configurations generated by both the parton shower and the matrix-element calculation.

To study the effect of different fixed order calculations and matching schemes, samples of top pair events were generated using the MC@NLO [18] and POWHEG [19] generators. The MC@NLO sample was produced with the CT10 [20] PDF set, and interfaced to HERWIG for the parton shower. The POWHEG sample was produced with the CTEQ6.6 PDF set and showered with the AUET2B-CTEQ6L1 PYTHIA [21] tune [22]. For each sample showered with HERWIG, JIMMY [23] was used for the underlying event simulation with the AUET1 tune [24]. To assess the effect of different parton shower models, a sample was generated using ALPGEN v2.14 with the PYTHIA parton shower and CTEQ5L PDF [25]. ISR/FSR variations were produced by varying the ALPGEN renormalisation scale associated

[2] $m_{\mathrm{T}}(W)$ is defined as $\sqrt{2p_{\mathrm{T}}^{l}p_{\mathrm{T}}^{\nu}(1-\cos(\phi^{l}-\phi^{\nu}))}$, where l and ν refer to the charged lepton (e or μ) and neutrino terms respectively. In the event selection the neutrino terms were replaced with $E_{\mathrm{T}}^{\mathrm{miss}}$ and its associated azimuthal angle ϕ.

with α_S in the matrix element calculation by a factor of two relative to the original scale k_T between two partons (setting the `ktfac` parameter to 0.5 and 2.0). These ISR/FSR variations were implemented by changing the α_S within the ME calculation while keeping the α_S used for the PDF and parton shower fixed, and are referred to as α_S-up (`ktfac` 0.5) and α_S-down (`ktfac` 2.0) variations within the rest of this note. The ALPGEN+PYTHIA nominal and α_S variation samples were made with the PYTHIA Perugia 2011 tune [26, 27]. These settings were shown to produce variations which enclose the uncertainty band of the $t\bar{t}$ jet veto measurement [5] (see Appendix A). In all samples a top quark mass of 172.5 GeV was assumed. All $t\bar{t}$ signal MC samples were normalised to a predicted $t\bar{t}$ cross-section of $\sigma_{t\bar{t}} = 167^{+17}_{-18}$ pb for a top quark mass of 172.5 GeV, as obtained from approximate NNLO QCD calculations [28].

Background samples of W and Z boson production with zero to four exclusive and five inclusive associated light partons were generated with ALPGEN v2.13 using CTEQ6L1 PDF, interfaced with the HERWIG parton shower. Since this analysis requires at least one jet to be identified as a b-quark jet, separate samples of $W + b\bar{b}$ + jets, $W + c$ + jets, $W + c\bar{c}$ + jets, and $Z + b\bar{b}$ + jets events were generated. The overlap between these samples and the respective inclusive jet flavour samples was removed using angular matching. In the case of W+jets, the normalisation was taken from a data-driven method.

The t-channel single top-quark sample was generated with the AcerMC generator [29], whereas MC@NLO was used to generate events in the Wt and s channels. The single top-quark samples were each normalised according to an approximate NNLO calculation of the t-channel ($64.6^{+2.6}_{-1.7}$ pb) [30], s-channel ($4.6^{+0.2}_{-0.2}$ pb) [31] and Wt-channel ($15.7^{+1.2}_{-1.2}$) [32] cross sections. Diboson events (WW, WZ, ZZ) were produced using HERWIG.

To simulate the effect of multiple in-time and out-of-time inelastic pp interactions, all MC events were overlaid with additional inelastic events generated with the PYTHIA AMBT1 tune, and re-weighted to match the distribution of the average number of additional interactions per bunch crossing in the data.

The resulting generated samples were passed through a GEANT4 [33] simulation of the ATLAS detector [34], except the ALPGEN+PYTHIA α_S up and down samples, which were passed through a fast simulation of the ATLAS detector. Events were then reconstructed in the same manner as the data.

5 Background estimation

The dominant background in this measurement is the associated production of W bosons with jets (including charm and bottom quarks), followed by QCD multijet production and single top-quark production. Smaller backgrounds arise from Z+jets and diboson production (WW, WZ, ZZ).

The overall normalisation of the W+jets contribution was extracted from a lepton charge asymmetry measurement from data:

$$N_{W^+} + N_{W^-} = \frac{r_{MC} + 1}{r_{MC} - 1}(D^+ - D^-) \ , \tag{1}$$

where $r_{MC} \equiv \frac{\sigma(pp\to W^+)}{\sigma(pp\to W^-)}$, D^+ (D^-) is the number of events in data with a positively (negatively) charged lepton, and N_{W^+} (N_{W^-}) is the number of W^+ (W^-) events. The normalisation was determined in W+jets events before any b-tagging requirement, separately for the W+3 jet, W+4 jet and $W+\geq 5$ jet events.

A data-driven approach was developed to measure the relative fractions of W bosons with jets of different heavy flavours using samples with two jets in the final state. The number of W+jets events after b-tagging can be expressed in terms of the number of W+jets events before b-tagging, the flavour fractions and b-tagging probabilities. The number of W+2 jet events before and after b-tagging were measured using the charge asymmetry technique and the flavour fractions were adjusted to ensure that the derived number of W+2 jet events after b-tagging matched the data. The overall charge-asymmetry normalisation was fixed, and a fit procedure was used to extract the normalisation of the bottom and charm quark fractions ($Wb\bar{b}$+jets, $Wc\bar{c}$+jets, and Wc+jets). The heavy flavour components were then extrapolated to events with higher jet multiplicities.

In the e + jets channel, either jets or electrons originating from photon conversions can mimic an isolated electron from the W decay. In the μ + jets channel this background is mostly from leptonic decays of heavy flavour quarks. The shape and normalisation of the QCD multijet background in the e + jets channel was obtained using a matrix method [35, 36] with looser electron identification cuts and no requirement on isolation of the electron. The $E_{\mathrm{T}}^{\mathrm{miss}} < 20$ GeV region was used as the control region for this method. The QCD multijet background in the μ + jets channel was determined using the mean of two matrix method estimates, which differ in their choice of control region. The first method uses a low $m_{\mathrm{T}}(W)$ region and the second method defines its control region by events in which the muon has a large impact parameter with respect to the primary vertex.

Contributions from single top, Z+jets, and diboson production were evaluated using the corresponding MC samples and theoretical cross sections for these processes.

6 Systematic uncertainties at reconstruction level

Systematic uncertainties were evaluated on the background and the signal predictions. The sources of systematic uncertainty are the object reconstruction and identification, the jet energy scale (JES) calibration, the jet energy resolution (JER), the b-tagging calibration, the QCD multijet background normalisation, and MC generator modelling.

Jet energy scale The total JES uncertainty takes into account in-situ measurements combined with additional uncertainties for close-by jets, the effects of multiple proton-proton interactions, and the flavour composition (light quark versus gluon) [11, 37, 38]. The assumed quark-gluon flavour fractions in the JES uncertainty evaluation were evaluated using the ALPGEN+HERWIG and MC@NLO $t\bar{t}$ signal samples for each jet multiplicity (from three to seven jets) individually. For events with more than seven jets, the uncertainty evaluated for seven-jet events was used. For jets within the acceptance, the JES uncertainty was found to vary in the range 1.5–8% depending on jet p_{T}, η, and the jet multiplicity in the event. An additional p_{T}-dependent uncertainty of $< 2.5\%$ was applied to jets matched to b-hadrons, and was added in quadrature to the JES uncertainty.

Jet energy resolution The measurements of jet energy resolution (JER) from MC simulation and data were found to agree [11]. The uncertainty on the JER was evaluated by smearing jets according to the systematic uncertainties on its measurement. The jets were smeared by 2-20%, depending on p_{T} and η.

Jet reconstruction efficiency The jet reconstruction efficiency was measured as the fraction of jets reconstructed from tracks in the ID that were matched to a calorimeter jet. The difference observed between data and MC simulation was taken as a systematic uncertainty, which was applied to the simulation by randomly removing a fraction of selected jets. The difference was at most 3% at low jet p_{T} [11].

***b*-tagging** The efficiency of the b-tagging algorithm was measured from data in QCD multijet samples and $t\bar{t}$ samples with several calibration methods, and from the difference between data and MC efficiencies, p_{T} and η-dependent scale factors were derived and applied to the MC events. The uncertainties on the scale factors were derived from the statistical and systematic uncertainties on the efficiency measurements [39].

The mis-tag scale factors for charm and light jets were measured using a vertex mass method. The vertex mass was constructed from the invariant mass of the charged particles associated with the secondary vertex. Templates were derived from simulations and fitted to the vertex mass distribution ob-

tained from data after applying the b-tagging. The c-jet efficiencies were measured with an analysis based on D^* mesons.

Jet primary vertex requirement The per-jet efficiency of the JVF > 0.75 requirement was measured in $Z(\rightarrow l^+l^-)$ + 1-jet events with a suppressed content of jets from additional primary interactions. This suppression was achieved by selecting events where the jet is back-to-back to the Z boson, with matching recoil transverse momentum. The systematic uncertainty due to the JVF requirement was estimated by varying the selection parameters used to define the Z + 1-jet region, and from fit uncertainties within the nominal region.

Leptons The mis-modelling of lepton trigger, reconstruction and selection efficiencies in the simulation were corrected for by scale factors derived from measurements of these efficiencies in data. Z and W boson decays ($Z \rightarrow \mu\mu$, $Z \rightarrow ee$, and $W \rightarrow e\nu$) were used to obtain scale factors as functions of the lepton kinematics.

Missing transverse energy The missing transverse energy calculation included energy scale and resolution corrections for leptons and jets. For the calorimeter cells not associated with a reconstructed lepton or jet with p_{T} greater than 20 GeV, an uncertainty dependent on the ΣE_{T}, the total transverse energy in the calorimeters, was assigned to their energy. This is referred to as the "Cell Out" uncertainty. The uncertainty on $E_{\mathrm{T}}^{\mathrm{miss}}$ due to additional pp interactions was calculated by varying the soft jet (cells associated with jets with $7 < p_{\mathrm{T}} < 20$ GeV), and Cell Out components of $E_{\mathrm{T}}^{\mathrm{miss}}$ by 6.6%, estimated by studying the dependence of ΣE_{T} on the number of pile-up interactions.

Generator model dependencies The associated uncertainty of selecting the CTEQ6L1 PDF for the generation the $t\bar{t}$ ALPGEN MC sample was evaluated by using the PDF set MSTW2008lo68cl [40] and its corresponding uncertainty set, to re-weight the $t\bar{t}$ MC sample. The systematic uncertainty was determined from the sum in quadrature of the differences obtained using the MSTW2008lo68cl PDF eigenvector sets as well as the difference between the results based on the best-fit PDF sets of MSTW2008lo68cl and CTEQ6L1.

The uncertainty due to the parton shower modelling was determined by taking the difference between the reconstructed yield from the ALPGEN+HERWIG $t\bar{t}$ sample and the central ALPGEN+PYTHIA $t\bar{t}$ MC sample.

The uncertainty from ISR/FSR variations was estimated by taking the maximum difference between the reconstructed yields from the central ALPGEN+PYTHIA $t\bar{t}$ sample and the ALPGEN+PYTHIA α_{S}-up and α_{S}-down $t\bar{t}$ samples.

The difference between fixed order matrix element calculations and associated matching schemes was estimated by comparing the POWHEG+PYTHIA $t\bar{t}$ sample with ALPGEN+PYTHIA. This sample was chosen in preference to MC@NLO, since MC@NLO was found not to describe the data in higher jet multiplicity bins ($\geq$ 6 jets).

***W*+jets modelling** The uncertainty on the W+jets normalisation scale factors derived from the charge asymmetry technique varied from 7% in 3-jet events up to 15% in $\geq$ 5-jet events. This includes reconstruction, charge misidentification, backgrounds, MC generator uncertainties and PDF variations. The uncertainty on the heavy flavour fractions includes reconstruction, background and MC generator uncertainties and an additional uncertainty of 25% in scaling from the 2-jet bin to any higher jet multiplicity. The uncertainty on the shape of the W+jets MC distribution was estimated by varying the factorisation and renormalisation scales (`iqopt3` in ALPGEN) and the generator cuts (`ptjmin` in ALPGEN).

QCD multijet modelling The shape uncertainty on the QCD multijet background in the electron channel was estimated by varying the maximum $E_{\mathrm{T}}^{\mathrm{miss}}$ requirement for the control region between 15 and 25 GeV. The shape uncertainty in the muon channel was taken from the difference between the mean and individual shapes. The normalisation uncertainties were taken to be 50% and 20% for the electron and muon channels respectively, where the normalisation uncertainty in the muon channel was estimated from the comparison of the two muon channel control regions.

Other theoretical uncertainties The theoretical uncertainty on the single top cross-section was taken from the approximate NNLO cross-section uncertainties as 4% (t-channel), 4% (s-channel) and 8% (Wt-channel). The theoretical uncertainty on the diboson cross-section was taken to be 5%, and for Z+jets $4\% \oplus 24\%$ per jet was used.

Luminosity The integrated luminosity was measured from van der Meer scans and was used to normalise several of the MC samples. The systematic uncertainty on this measurement was estimated to be 3.9% [41][3]. This uncertainty was applied to all MC simulation signals and backgrounds, but not to the data-driven W+jets and QCD multijet backgrounds.

7 Reconstructed yields and distributions

A summary of the number of selected data events, expected $t\bar{t}$ signal events and background contributions is given in Table 1. The predicted and observed reconstructed jet multiplicity for the jet p_{T} thresholds 25, 40, 60 and 80 GeV is illustrated in Figures 1 and 2. The predictions of the ALPGEN+HERWIG $t\bar{t}$ simulation plus background estimates agree with the observed jet multiplicity spectra.

8 Corrections and unfolding to particle level

8.1 Particle-level selection and kinematic range

The present measurements were fully corrected to a kinematic range closely matching the acceptance of the event selection applied to reconstructed objects described in Section 3.

In the MC simulation, stable particles were defined by requiring a lifetime $\tau > 0.3 \times 10^{-10}$ s. Generated electrons were dressed with prompt photons found within a cone of radius $\Delta R = 0.1$ around their direction. This dressing is similar to the effect of the spatial resolution of the calorimeter and the electron energy clustering algorithm. The dressed electrons were required to have $p_{\mathrm{T}} > 25$ GeV, and $|\eta| < 2.47$, excluding the barrel/end-cap transition region of $1.37 < |\eta| < 1.52$. Simulated muons were required to have $p_{\mathrm{T}} > 25$ GeV and pseudorapidity $|\eta| < 2.5$.

Electrons, muons and neutrinos were required to be decay products of generated W bosons, either directly or via a leptonic tau decay. The vector sum of the generated neutrino four momenta was used to compute $E_{\mathrm{T}}^{\mathrm{miss}}$ and the corresponding azimuthal angle.

With the exception of neutrinos and muons, stable particles were clustered into particle jets using the anti-k_t algorithm with a radius parameter of 0.4. Particles from the underlying event were included in this definition, whereas particles from overlaid inelastic events were not. Particle jets were required to be within the pseudorapidity range $|\eta| < 2.5$ and have a transverse momentum $p_{\mathrm{T}} > 25$ GeV. This transverse momentum threshold was then raised to match each of the other jet p_{T} thresholds considered. Particle

[3] An uncertainty of 3.9% is used – as opposed to the 3.7% of Ref. [41] – due to slightly larger uncertainties in the second half of 2011 data taking.

Electron channel						
Source	$n_{\text{jets}}^{\text{reco}}$=3	$n_{\text{jets}}^{\text{reco}}$=4	$n_{\text{jets}}^{\text{reco}}$=5	$n_{\text{jets}}^{\text{reco}}$=6	$n_{\text{jets}}^{\text{reco}}$=7	$n_{\text{jets}}^{\text{reco}}\geq$8
$t\bar{t}$	9800±1100	9600±1300	4900±1100	2000±600	590±270	220±130
W+jets	5300±1300	1700±400	440±140	100±30	20±7	7±2
QCD multijet	1900±900	800±400	350±180	120±60	32±16	15±8
single top	1980±230	820±120	240±50	58±16	13±5	2±2
Z+jets	610±80	260±60	99±23	25±11	7±2	1±2
Diboson	150±60	35±14	7±3	1.2±0.6	0.19±0.19	0.11±0.11
Expectation	19800±2000	13200±1500	6100±11200	2200±600	700±270	250±140
Data	20320	12704	5632	1856	566	188

Muon channel						
Source	$n_{\text{jets}}^{\text{reco}}$=3	$n_{\text{jets}}^{\text{reco}}$=4	$n_{\text{jets}}^{\text{reco}}$=5	$n_{\text{jets}}^{\text{reco}}$=6	$n_{\text{jets}}^{\text{reco}}$=7	$n_{\text{jets}}^{\text{reco}}\geq$8
$t\bar{t}$	11500±1200	11100±1200	5900±1100	2300±700	720±300	250±170
W+jets	7300±1500	2300±500	560±160	120±28	30±7	11±3
QCD multijet	2200±500	800±160	300±60	85±17	20±5	11±2
single top	2360±250	970±130	290±50	70±18	10±5	4±1
Z+jets	380±70	140±30	50±10	14±5	1±3	0.5±0.7
Diboson	170±70	41±16	7±3	1.2±0.6	0.0±0.3	0.13±0.17
Expectation	24000±2000	15400±1300	7100±1100	2600±700	780±300	280±170
Data	24422	15162	6578	2348	722	252

Table 1: Event yields for data and MC simulation in the electron and muon channels, selected with a 25 GeV jet p_{T} threshold. The number of events passing all selection requirements are shown as a function of the reconstructed jet multiplicity ($n_{\text{jets}}^{\text{reco}}$). ALPGEN+HERWIG is used for the $t\bar{t}$ simulation and MC expectations are normalised to 4.7 fb^{-1}. The uncertainties on the expected values include all systematic uncertainties discussed in Section 6, as well as the statistical uncertainties of each of the samples. The W+jets and QCD multijet background estimations are data-driven. The $t\bar{t}$ modelling uncertainties were evaluated from their relative shifts.

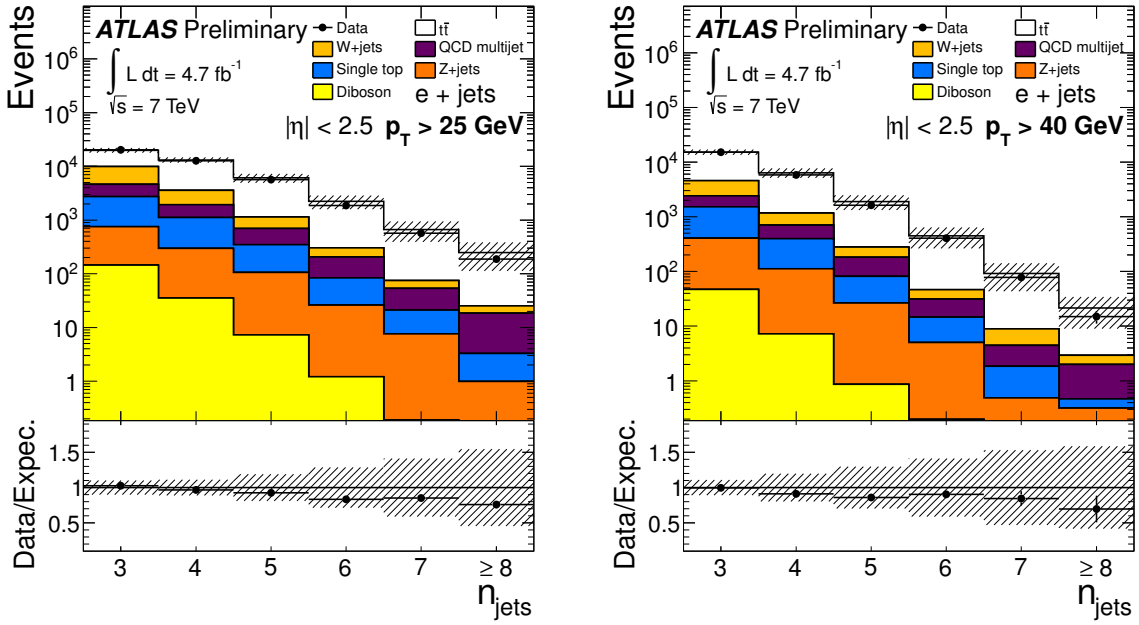

(a) $p_{\mathrm{T}} > 25$ GeV

(b) $p_{\mathrm{T}} > 40$ GeV

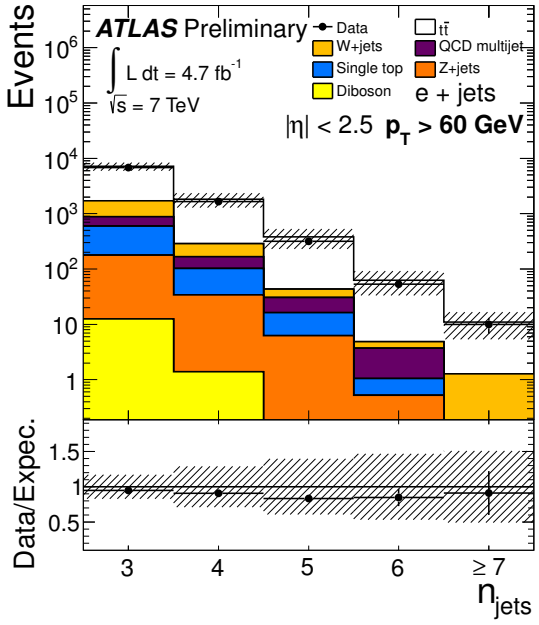

(c) $p_{\mathrm{T}} > 60$ GeV

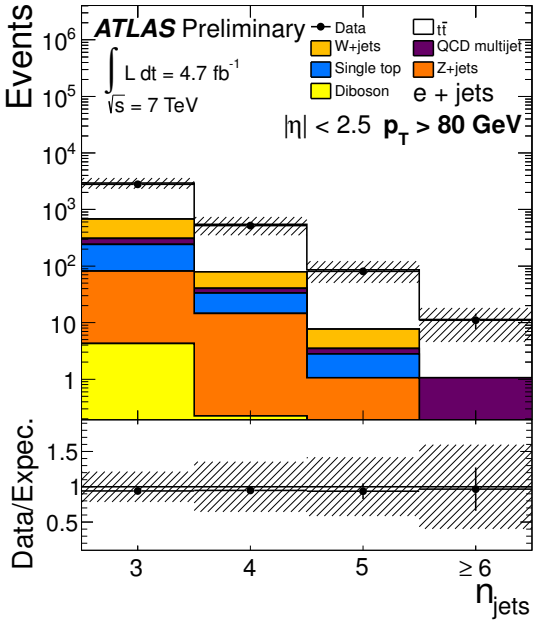

(d) $p_{\mathrm{T}} > 80$ GeV

Figure 1: The reconstructed jet multiplicities for the electron channel and the jet p_{T} thresholds (a) 25, (b) 40, (c) 60, and (d) 80 GeV. The data are shown compared to the sum of the MC signal, MC background and data driven background models. ALPGEN+HERWIG MC is used for the $t\bar{t}$ signal estimate. The shaded band shows the total systematic and statistical uncertainties on the signal plus background estimate.

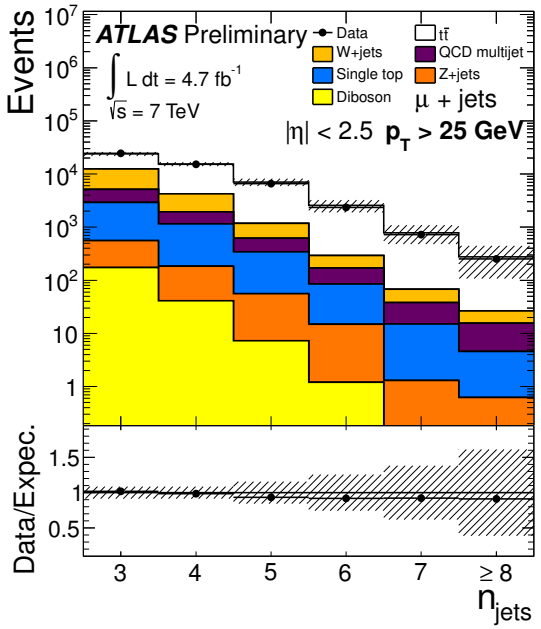

(a) $p_{\mathrm{T}} > 25$ GeV

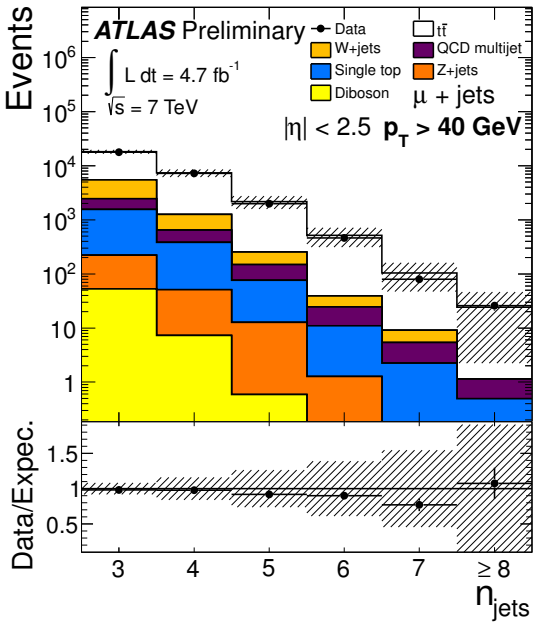

(b) $p_{\mathrm{T}} > 40$ GeV

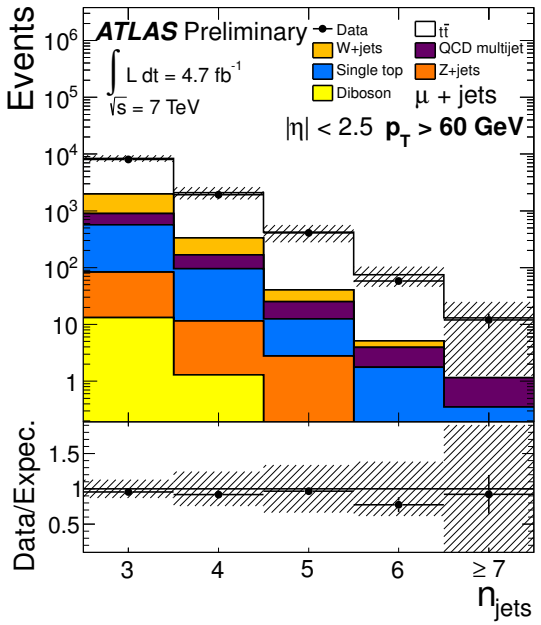

(c) $p_{\mathrm{T}} > 60$ GeV

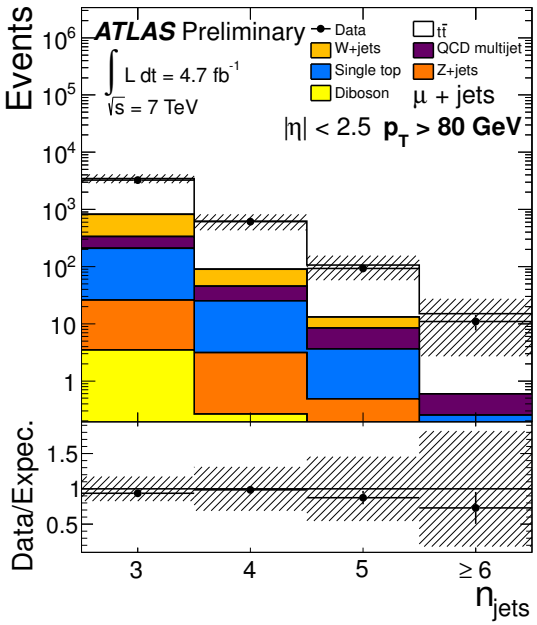

(d) $p_{\mathrm{T}} > 80$ GeV

Figure 2: The reconstructed jet multiplicities for the muon channel and the jet p_{T} thresholds (a) 25, (b) 40, (c) 60, and (b) 80 GeV. The data are shown compared to the sum of the MC signal, MC background and data driven background models. ALPGEN+HERWIG MC is used for the $t\bar{t}$ signal estimate. The shaded band shows the total systematic and statistical uncertainties on the signal plus background estimate.

jets were b-tagged by requiring at least one $\Delta R < 0.3$ match between a b-hadron with $p_{\mathrm{T}} > 5$ GeV and the particle jet.

For each dressed electron, the closest particle jet within a $\Delta R < 0.2$ was removed. For the purpose of this overlap removal for particle jets, electrons down to a p_{T} of 15 GeV were considered. All selected muons overlapping with particle jets within a cone of $\Delta R < 0.4$ were discarded.

The fiducial range of this measurement was defined by the presence of exactly one lepton (muon or dressed electron), at least three particle jets, $E_{\mathrm{T}}^{\mathrm{miss}} > 30$ GeV and a transverse W mass greater than 35 GeV. The additional lepton (muon or dressed electron) veto was applied down to a p_{T} of 15 GeV.

8.2 Correction procedure

The reconstructed jet multiplicity spectrum was corrected back to the particle-level within the selected kinematic range, by accounting for detector efficiencies, resolution effects and biases. The data were correcting according to,

$$\vec{N}_{\mathrm{part}} = \vec{f}_{\mathrm{part!reco}} \cdot \mathbf{M}_{\mathrm{part}}^{\mathrm{reco}} \cdot \vec{f}_{\mathrm{reco!part}} \cdot \vec{f}_{\mathrm{accpt}} \cdot (\vec{N}_{\mathrm{reco}} - \vec{f}_{\mathrm{bgnd}}) \tag{2}$$

where N_{reco} is the total number of reconstructed events, f_{bgnd} is the background contribution discussed in Section 5, f_{accpt} is an acceptance correction for all selection efficiencies except for the jet multiplicity requirement, $f_{\mathrm{reco!part}}$ is a correction for events passing the jet multiplicity requirement at the reconstruction level but not at the particle level, $\mathbf{M}_{\mathrm{part}}^{\mathrm{reco}}$ is a response matrix applied iteratively using Bayesian unfolding [42], $f_{\mathrm{part!reco}}$ is an efficiency correction factor correcting for events which fulfil the particle-level jet multiplicity requirement, but fail the same at the reconstruction level and N_{part} is the total number of fully corrected events. The total number of reconstructed events N_{reco} and the correction factors f_{bgnd}, f_{accpt}, and $f_{\mathrm{reco!part}}$ are functions of the reconstructed jet multiplicity $n_{\mathrm{jets}}^{\mathrm{reco}}$. The total number of fully corrected events N_{part} and the efficiency factor $f_{\mathrm{part!reco}}$ are functions of the particle jet multiplicity $n_{\mathrm{jets}}^{\mathrm{part}}$.

The correction factor $f_{\mathrm{reco!part}}$ and the matrix $\mathbf{M}_{\mathrm{part}}^{\mathrm{reco}}$ were defined for the reconstructed multiplicity after the correction for all non-jet acceptance effects. To calculate these factors and the numerator of f_{accpt}, the reconstructed jet multiplicity was counted after the removal of jets which overlapped with dressed electrons. Any jet found to match with a dressed electron from a generated W boson was discarded. The resulting jet multiplicity for all events which passed particle-level lepton and b-tagging requirements was used for one dimension of $\mathbf{M}_{\mathrm{part}}^{\mathrm{reco}}$, and the f_{accpt} numerator. The $f_{\mathrm{reco!part}}$ parameter was taken from $\mathbf{M}_{\mathrm{part}}^{\mathrm{reco}}$ before the removal of entries with less than three particle or reconstructed jets. The $f_{\mathrm{part!reco}}$ parameter was derived from the $\mathbf{M}_{\mathrm{part}}^{\mathrm{reco}}$ matrix, using the probability of three reconstructed jets given four particle jets.

The f_{accpt} factor was found to be 1.8–1.9 for the electron channel and 1.4–1.5 for the muon channels, where the lower values correspond to the highest jet p_{T} thresholds and the distribution for a given threshold is flat within the statistical uncertainties. The higher f_{accpt} value in the electron channel corresponds to the electron identification efficiency being lower than that of the muon identification. The value of $f_{\mathrm{reco!part}}$ for three reconstructed jets was found to vary between 0.9–0.75 for low to high jet multiplicity thresholds, in the electron and muon channels. The factor $f_{\mathrm{reco!part}}$ was found to be consistent with unity for all jet p_{T} thresholds when five or more jets were reconstructed. The diagonal elements of the response matrix $\mathbf{M}_{\mathrm{part}}^{\mathrm{reco}}$ were found to have values ranging from 0.5–0.9, where the diagonal elements {4,4} to {N,N} were within the range 0.5–0.7. The correction factor $f_{\mathrm{part!reco}}$ for three particle jets was found to vary within the range 0.9–0.75 for lower to higher jet p_{T} thresholds, in the same manner for electron and muon channels. The factor $f_{\mathrm{part!reco}}$ was found to be consistent with unity for all jet p_{T} thresholds when five or more particle jets were present.

8.3 Propagation of uncertainties

The correction factors ($f_{\text{part!reco}}$, $\mathbf{M}^{\text{reco}}_{\text{part}}$, $f_{\text{reco!part}}$, and f_{accpt}) were determined using the nominal ALPGEN+HERWIG $t\bar{t}$ MC sample. The systematic uncertainty due to the statistical uncertainty on the size of the MC sample used to populate $\mathbf{M}^{\text{reco}}_{\text{part}}$, $f_{\text{reco!part}}$, and f_{accpt} was estimated by smearing the response matrix ($\mathbf{M}^{\text{reco}}_{\text{part}}$) and the correction factors ($f_{\text{reco!part}}$ and f_{accpt}) according to Poisson distributions and normal distributions respectively. For this estimate, 1000 pseudoexperiments were performed, smearing the three terms simultaneously. For each smeared $\mathbf{M}^{\text{reco}}_{\text{part}}$, the correction factor $f_{\text{part!reco}}$ was recalculated. The difference between the mean of all 1000 unfolded distributions and the true ALPGEN+HERWIG $t\bar{t}$ distribution was taken to be the bias, whereas the standard deviation was taken to be the systematic uncertainty due to the statistical uncertainty on the $\mathbf{M}^{\text{reco}}_{\text{part}}$, $f_{\text{reco!part}}$ and f_{accpt}.

The uncertainty on f_{bgnd} was determined at the reconstruction-level, by combining the component uncertainties according to their correlations. Correlations between flavour tagging modelling and the data-driven W+jets normalisation where treated conservatively, by assuming the total W+jets normalisation uncertainties to be uncorrelated with MC modelling uncertainties. The systematic uncertainty on the unfolded spectra from the background was evaluated by performing 1000 pseudoexperiments, following a normal distribution with a width matching the total uncertainty band. The square root of the variance of the unfolded spectra of the pseudoexperiments was taken as the uncertainty on the background.

Systematic uncertainties affecting the $t\bar{t}$ sample used to unfold the jet multiplicity spectrum were evaluated as relative bias. For each variation, a pair of particle and reconstruction-level spectra was generated. The bias was evaluated by performing 1000 pseudoexperiments, fluctuating the reconstructed input spectrum within its statistical uncertainty. Each pseudoexperiment was unfolded (using the correction factors derived from the nominal ALPGEN+HERWIG $t\bar{t}$ sample) and the bias was calculated from the difference between the mean and the true distribution. The systematic uncertainty estimation was taken from the relative bias, the difference between the bias evaluated with the ALPGEN+HERWIG $t\bar{t}$ sample and the bias evaluated using each reconstructed and true systematic uncertainty variation sample. This applies to all cases except the ALPGEN+PYTHIA α_{S} variations, where the relative bias between the ALPGEN+PYTHIA central and shifted samples was used, and the generator uncertainty where ALPGEN+PYTHIA and POWHEG+PYTHIA were compared. The uncertainty on the leading order matrix element calculation and matching scheme (the generator uncertainty) was estimated from the relative bias of unfolding the POWHEG+PYTHIA sample. The MC@NLO sample was not used for this uncertainty, since it does not describe the data well at higher jet multiplicities.

Each of the $t\bar{t}$ uncertainties was propagated individually and symmetrised before being combined. The JES uncertainty is 3–40%, from low to higher jet multiplicities and the 25 GeV jet p_{T} threshold. The JES uncertainty falls in the higher jet multiplicities bins for the higher jet p_{T} thresholds, to values of around 15%. For the 25 GeV jet p_{T} threshold, the background uncertainty is 18%(3%) for events with low(high) jet multiplicities. The ISR/FSR modelling uncertainty varies from 1–6%. The next most significant uncertainties are the matrix element generator and jet flavour tagging uncertainties. These uncertainties are of a similar magnitude to the ISR/FSR uncertainty. The systematic uncertainty from the MC statistical uncertainties on each on the correction factions is within the range 1-11% (25 GeV p_{T} threshold) and becomes significant (40%) in events with 7(6) jets for the 60(80) GeV p_{T} thresholds. Statistical uncertainties from the data do not become dominant in any region.

9 Results

The fully corrected particle-jet multiplicities for the jet p_{T} thresholds 25, 40, 60, and 80 GeV are shown in Figures 3 and 4, for the electron and muon channels, respectively, and compared to predictions from ALPGEN+HERWIG, ALPGEN+PYTHIA (α_{S}-down), MC@NLO+HERWIG and the POWHEG+PYTHIA

MC models. The α_S-down variation of ALPGEN+PYTHIA was selected for Figures 3 and 4, since it most closely describes the data of the three parameter variations considered. The predictions of the different ALPGEN+PYTHIA models (nominal as well as the α_S-up and α_S-down variations) are compared with data in Figures 5 and 6. The number of events shown in each of the distributions corresponds to an integrated luminosity of 4.7 ± 0.2 fb^{-1}.

For the lowest jet p_T threshold, all MC predictions agree well with the data in the three and four-jet multiplicity bins. POWHEG and MC@NLO have an NLO treatment of the $t\bar{t}$ final state, an LO treatment of the $t\bar{t}j$ final state, and a leading log treatment of any additional jets. MC@NLO is in agreement with the data for the 25 GeV jet p_T threshold, for events with jet multiplicities in the range 3–5. For higher jet p_T thresholds, there is agreement for events with three or four jets (40 and 60 GeV jet p_T threshold) and with events with three jets (80 GeV jet p_T threshold). However, MC@NLO underestimates the data for events with more than six jets and a jet p_T threshold of 25 GeV, and for events with lower jet multiplicities as the jet p_T threshold is increased. This indicates that the p_T spectrum predicted by MC@NLO is too soft. For a $t\bar{t}$ five jet final state, MC@NLO+HERWIG is known to underestimate the contribution of the $t\bar{t} + q(g)$ hard process (producing too much of the additional jet production from parton showering rather than from the tree-level matrix element) [43]. The underestimate of the higher jet multiplicity bins for MC@NLO compared to ALPGEN is also observed in Ref. [43]. The prediction from POWHEG+PYTHIA is in reasonable agreement with the data for all jet p_T thresholds and jet multiplicities.

With the exception of events with three or four jets (25 GeV jet p_T threshold) and three jets (40 GeV jet p_T threshold), the ALPGEN+PYTHIA α_S-up variation is found to generate higher jet multiplicities than observed in the data. The nominal ALPGEN+PYTHIA sample also diverges from the data for events with higher jet multiplicities and the jet p_T thresholds of 60 and 80 GeV. The predictions from ALPGEN+HERWIG and the ALPGEN+PYTHIA α_S-down variation are consistent with the data for all jet p_T thresholds.

10 Conclusions

Jet multiplicity spectra have been measured for 25, 40, 60, and 80 GeV jet p_T thresholds, from a pp data sample rich in single-lepton channel $t\bar{t}$ events. These spectra from an integrated luminosity of 4.7 ± 0.2 fb^{-1} have been fully corrected for detector effects and unfolded within a kinematic range closely matching the range used for the experimental measurement. The presented measurement is limited by systematic uncertainties, from background modelling (at lower jet multiplicities) to jet energy scale (at higher jet multiplicities). The presented data disfavour the MC@NLO model, which predicts a lower jet multiplicity spectrum and softer jets. The MC prediction from ALPGEN+PYTHIA with an upward α_S variation is found to be disfavoured the data. Predictions from ALPGEN showered with HERWIG or PYTHIA, and from POWHEG showered with PYTHIA are consistent with the data within the total uncertainties of the measurement.

A ALPGEN+PYTHIA ISR/FSR variations

The measurements presented in [5] were used to motivate the ALPGEN+PYTHIA α_S variations used for the ISR/FSR modelling systematic uncertainties. The measurements included a gap fraction (f_{gap}), which is the fraction of events with no additional jet radiated with a considered rapidity interval. The event selection required $t\bar{t}$ events with two leptons in the final state. Following this selection, two veto definitions were used: (i) where events were vetoed if they contain an additional jet in the considered rapidity interval with transverse momentum above a threshold (Q_0), and (ii) where events were vetoed if they contain a scalar sum of all additional jets in the given region above a threshold (Q_{sum}).

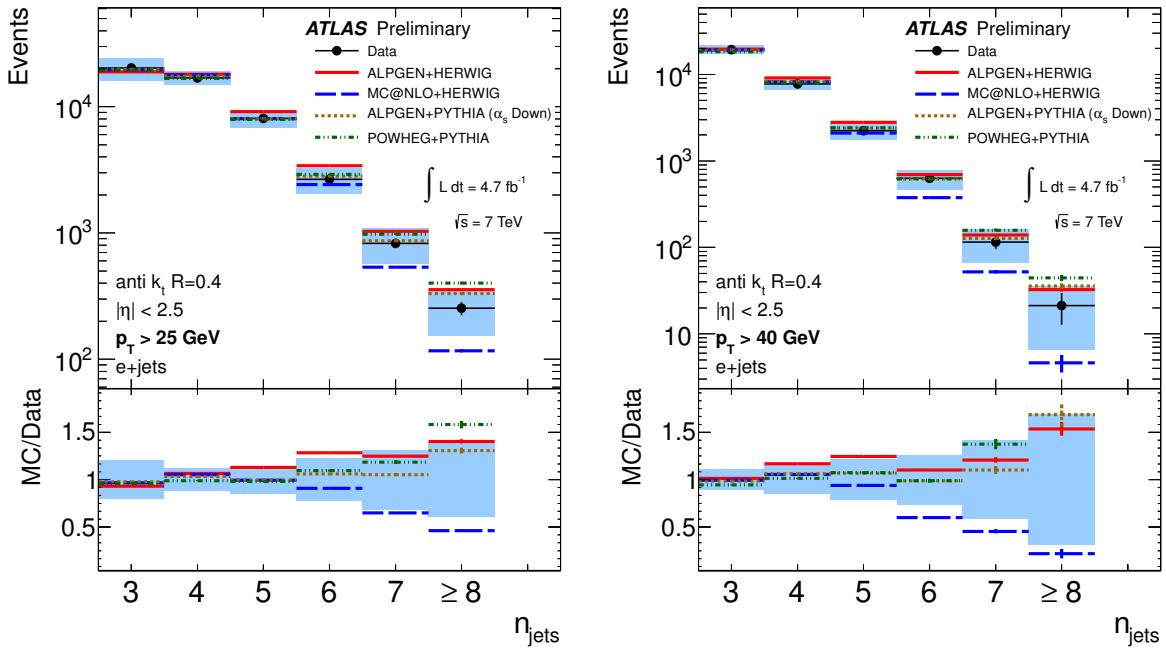

(a) $p_{\mathrm{T}} > 25$ GeV

(b) $p_{\mathrm{T}} > 40$ GeV

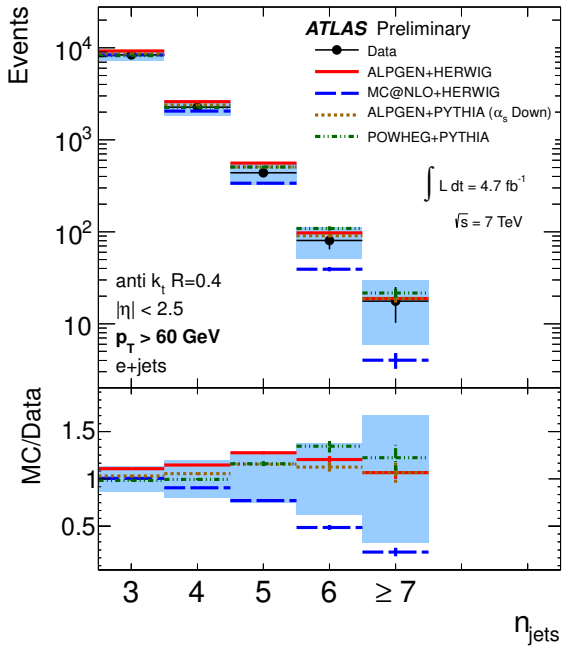

(c) $p_{\mathrm{T}} > 60$ GeV

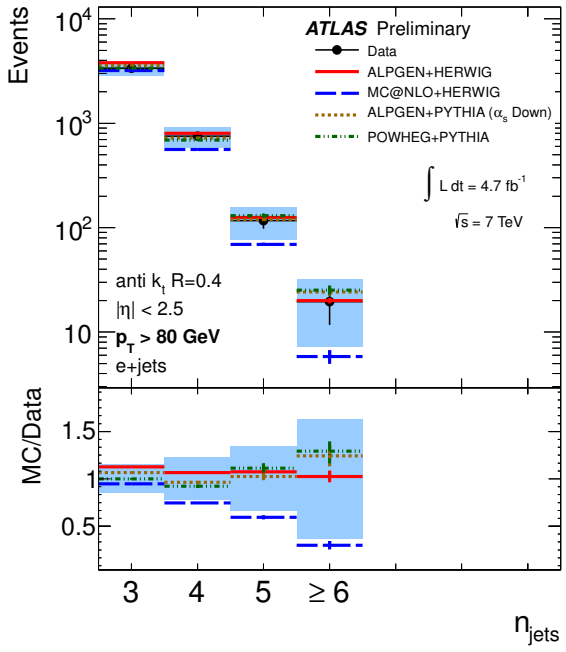

(d) $p_{\mathrm{T}} > 80$ GeV

Figure 3: The particle-jet multiplicities for the electron channel and the jet p_{T} thresholds (a) 25, (b) 40, (c) 60, and (d) 80 GeV. The data are shown in comparison to the ALPGEN+HERWIG, ALPGEN+PYTHIA (α_{S}-down variation), MC@NLO+HERWIG and POWHEG+PYTHIA MC models. The data points and their corresponding statistical uncertainty are shown in black, whereas the total uncertainty (syst. $\oplus$ stat.) is shown as a shaded band. The MC predictions are shown with their statistical uncertainty.

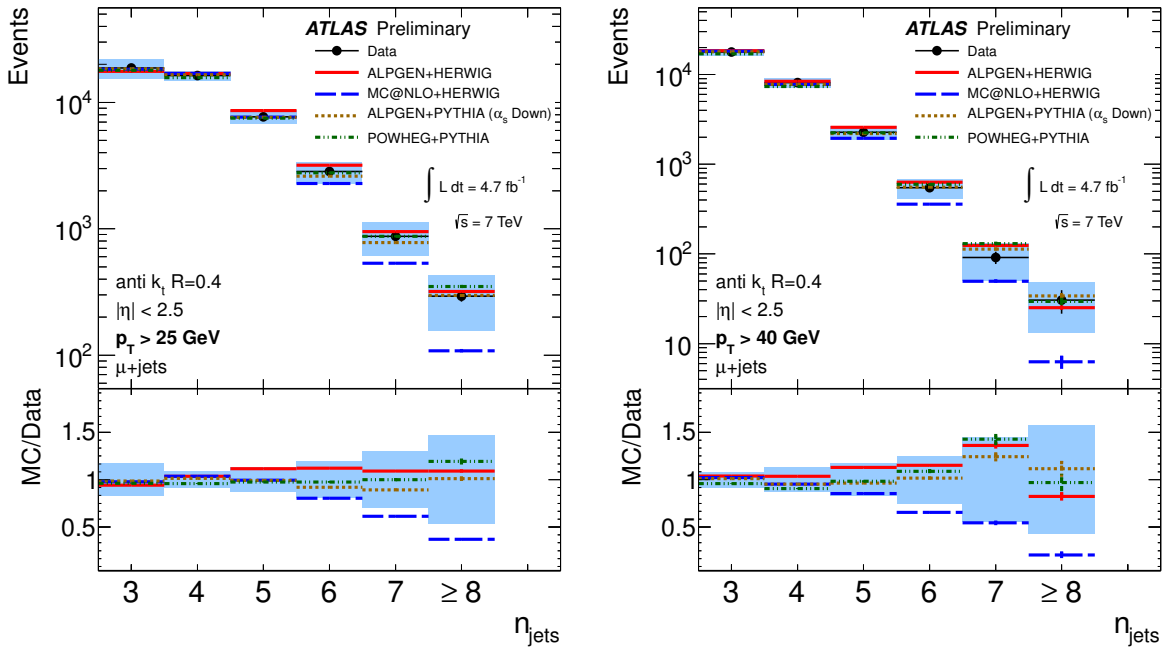

(a) $p_{\mathrm{T}} > 25$ GeV

(b) $p_{\mathrm{T}} > 40$ GeV

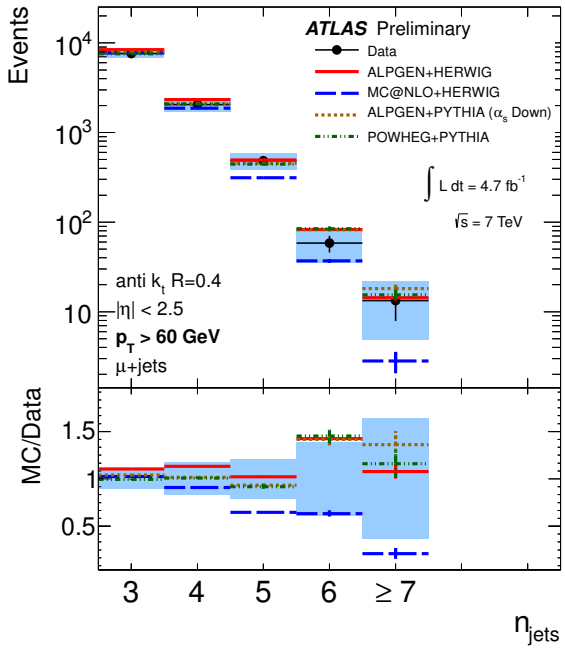

(c) $p_{\mathrm{T}} > 60$ GeV

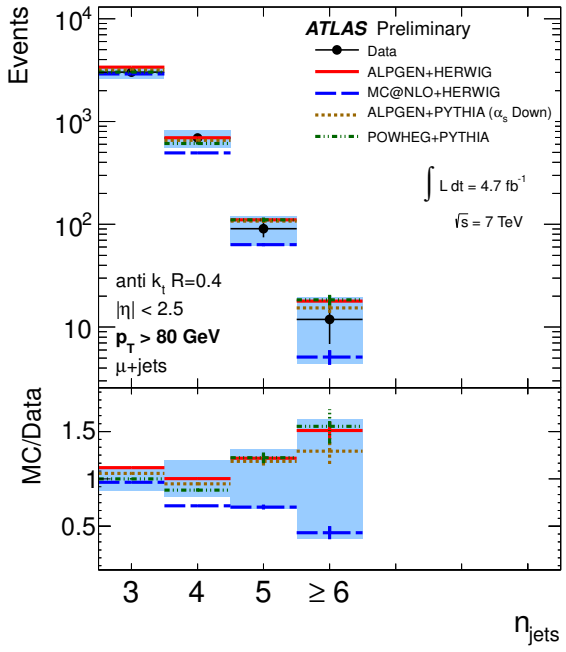

(d) $p_{\mathrm{T}} > 80$ GeV

Figure 4: The particle-jet multiplicities for the muon channel and the jet p_{T} thresholds (a) 25, (b) 40, (c) 60, and (d) 80 GeV. The data are shown in comparison to the ALPGEN+HERWIG, ALPGEN+PYTHIA (α_{S}-down variation), MC@NLO+HERWIG and POWHEG+PYTHIA MC models. The data points and their corresponding statistical uncertainty are shown in black, whereas the total uncertainty (syst. $\oplus$ stat.) is shown as a shaded band. The MC predictions are shown with their statistical uncertainty.

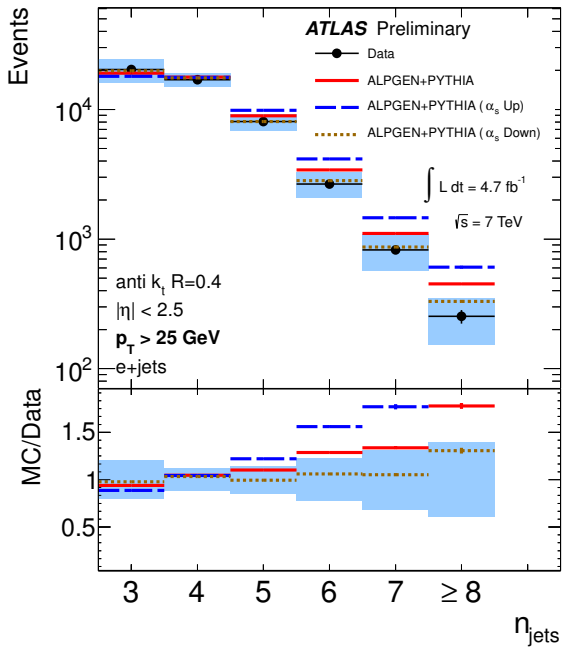

(a) $p_{\mathrm{T}} > 25$ GeV

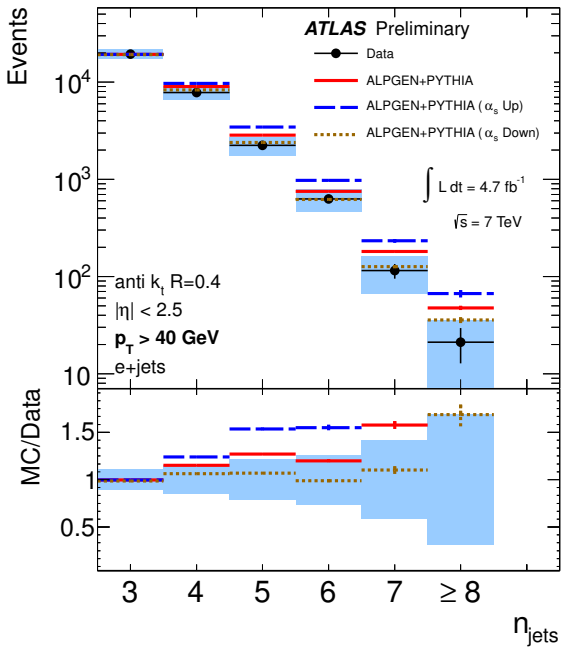

(b) $p_{\mathrm{T}} > 40$ GeV

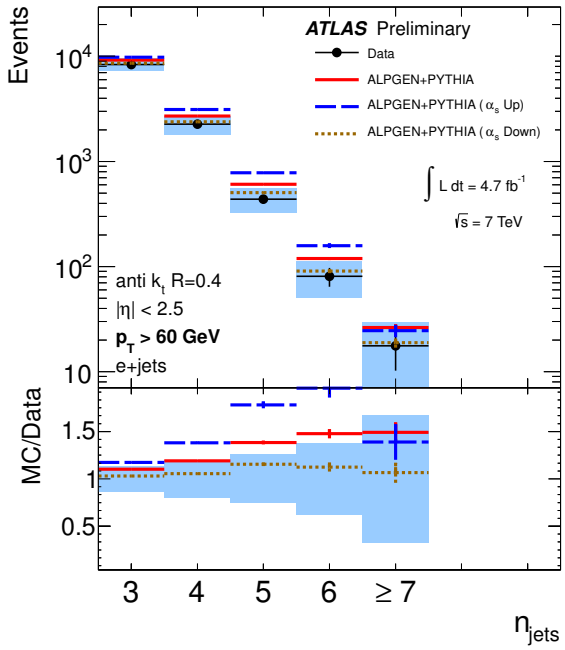

(c) $p_{\mathrm{T}} > 60$ GeV

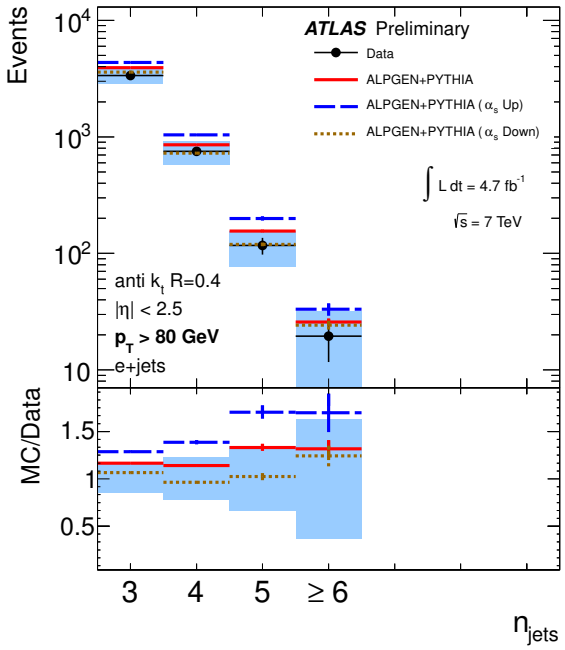

(d) $p_{\mathrm{T}} > 80$ GeV

Figure 5: The particle-jet multiplicities for the electron channel and the jet p_{T} thresholds (a) 25, (b) 40, (c) 60, and (d) 80 GeV. The data are shown in comparison to the ALPGEN+PYTHIA and ALPGEN+PYTHIA α_{S} variations. The data points and their corresponding statistical uncertainty are shown in black, whereas the total uncertainty (syst. $\oplus$ stat.) is shown as a shaded band. The MC predictions are shown with their statistical uncertainty.

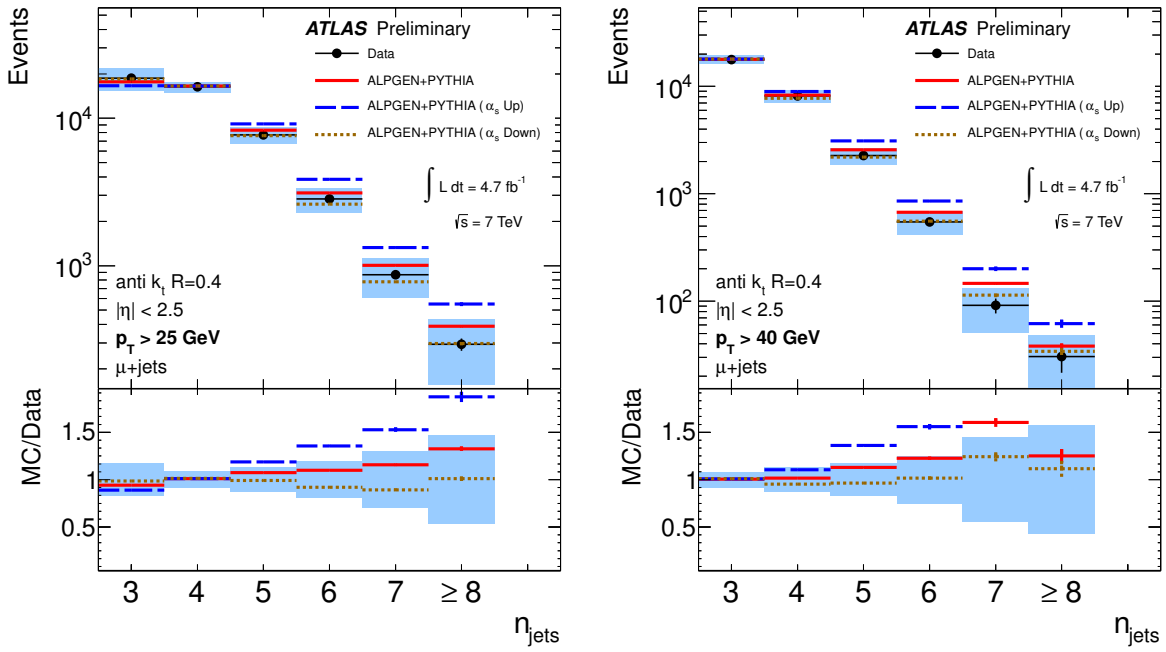

(a) $p_{\mathrm{T}} > 25$ GeV

(b) $p_{\mathrm{T}} > 40$ GeV

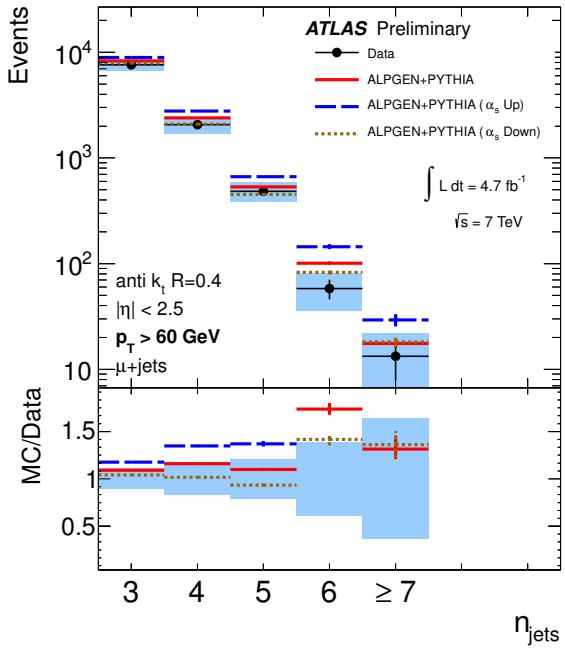

(c) $p_{\mathrm{T}} > 60$ GeV

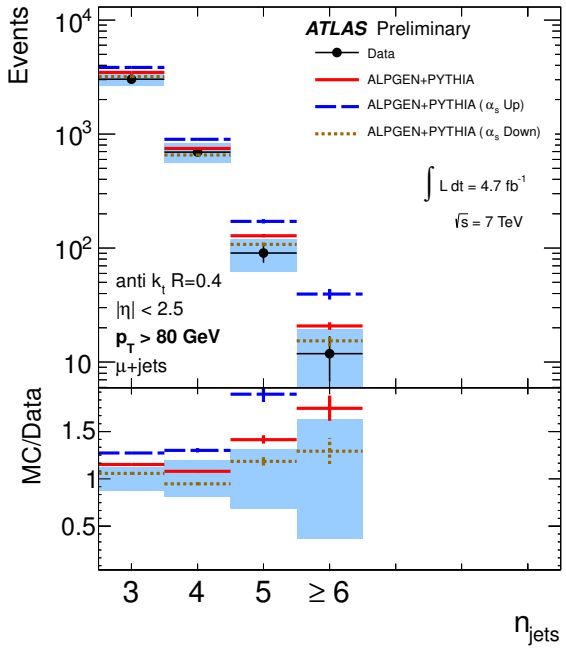

(d) $p_{\mathrm{T}} > 80$ GeV

Figure 6: The particle-jet multiplicities for the muon channel and the jet p_{T} thresholds (a) 25, (b) 40, (c) 60, and (d) 80 GeV. The data are shown in comparison to the ALPGEN+PYTHIA and ALPGEN+PYTHIA α_{S} variations. The data points and their corresponding statistical uncertainty are shown in black, whereas the total uncertainty (syst. $\oplus$ stat.) is shown as a shaded band. The MC predictions are shown with their statistical uncertainty.

Figures 7 and 8 compare the ALPGEN+PYTHIA α_S variations described within this note with the measured gap fraction of Ref. [5]. The variations provide an uncertainty band around the data. This is true for all regions with the exception of the most forward rapidity region, where all variations are below the data. Other MC generators were found to have a similar behaviour in the forward region [5]. The α_S-down variation is closest to the data and within the experimental uncertainty.

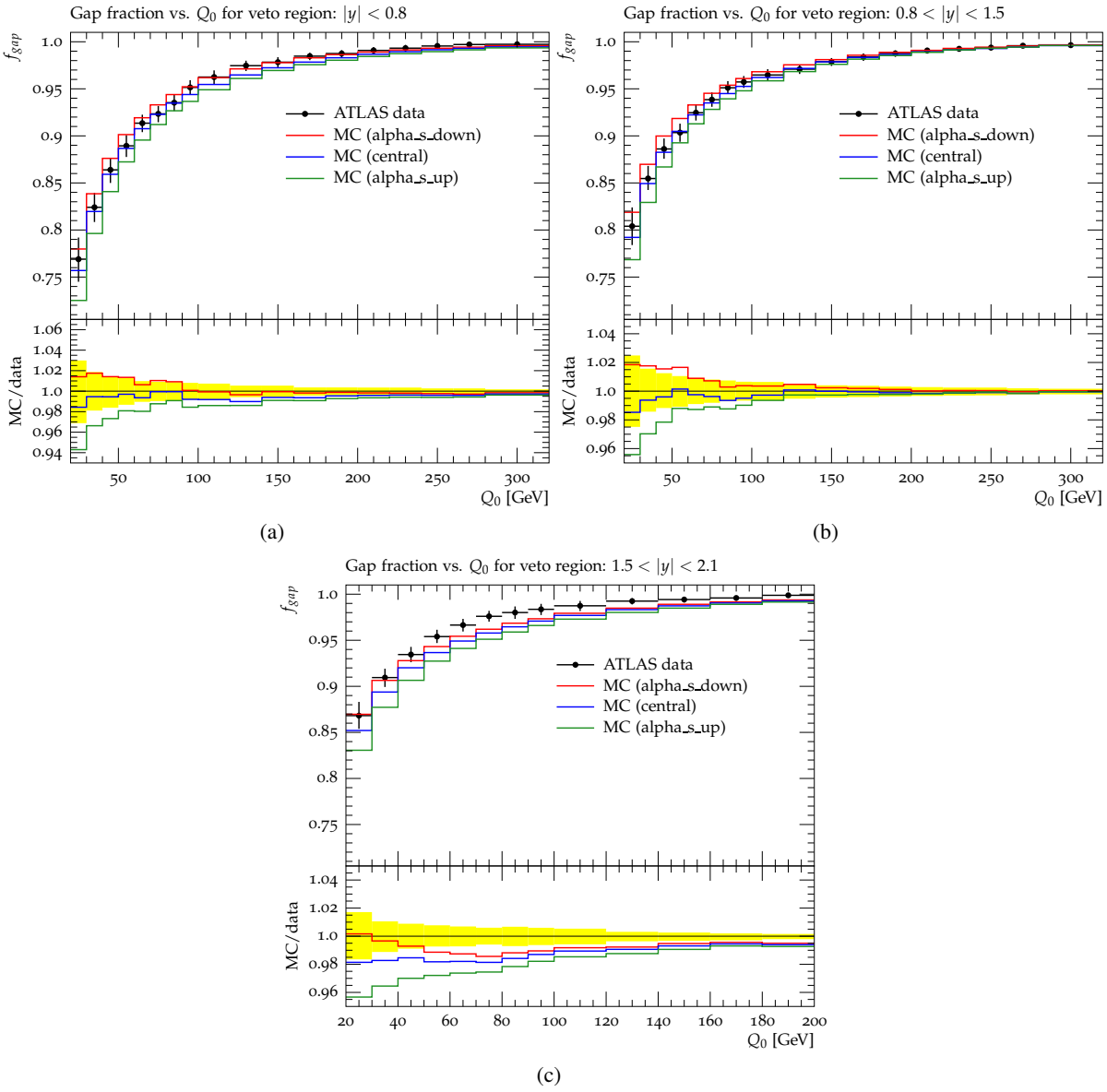

(a) (b)

(c)

Figure 7: ALPGEN+PYTHIA sample variations for the rapidity regions (a) $|y| < 0.8$, (b) $0.8 < |y| < 1.5$, and (c) $1.5 < |y| < 2.1$ compared to the measured gap fraction as a function of p_T threshold [5]. The central sample is shown together with the α_S-up and α_S-down variations.

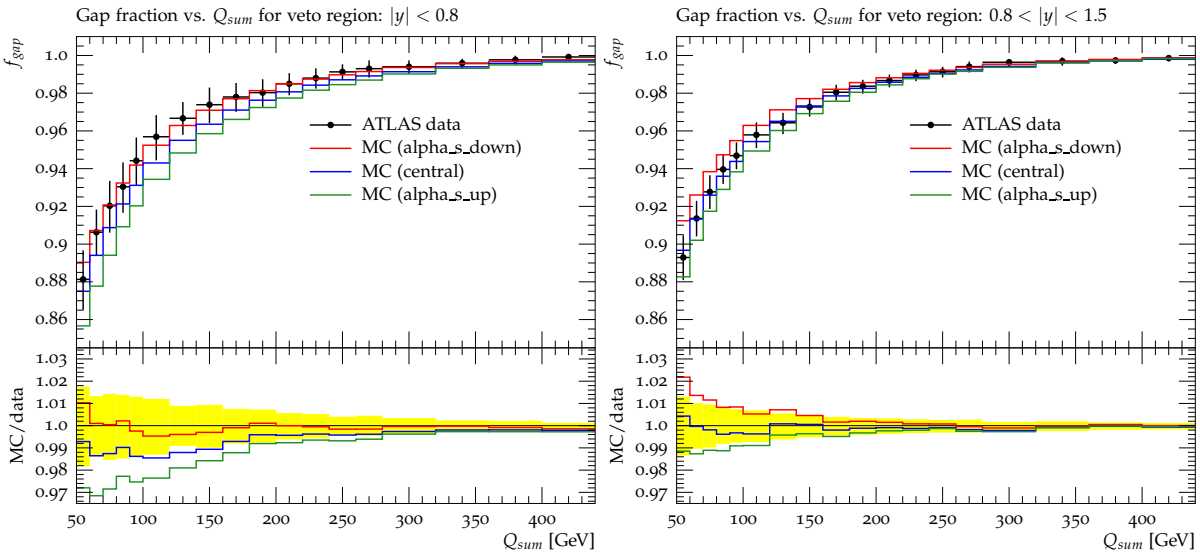

(a)

(b)

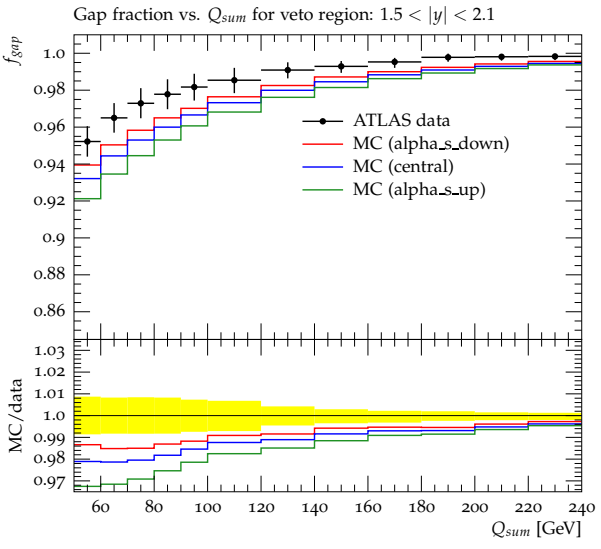

(c)

Figure 8: ALPGEN+PYTHIA sample variations for the rapidity regions (a) $|y| < 0.8$, (b) $0.8 < |y| < 1.5$, and (c) $1.5 < |y| < 2.1$ compared to the measured gap fraction as a function of the scalar sum of jets [5]. The central sample is shown together with the α_S-up and α_S-down variations.

References

[1] The ATLAS Collaboration, *Measurement of the $t\bar{t}$ production cross-section in pp collisions at $\sqrt{s}$ = 7 TeV using kinematic information of lepton+jets events*, ATLAS-CONF-2011-121.

[2] The ATLAS Collaboration, *Measurement of the cross section for top-quark pair production in pp collisions at $\sqrt{s}$ = 7 TeV with the ATLAS detector using final states with two high-p_{T} leptons*, JHEP **1205** (2012), 059.

[3] The CMS Collaboration, *Measurement of the $t\bar{t}$ Production Cross Section in pp Collisions at 7 TeV in Lepton + Jets Events Using b-quark Jet Identification*, Phys. Rev. **D84** (2011), 092004.

[4] The ATLAS Collaboration, *Reconstructed jet multiplicities from the top-quark pair decays and associated jets in pp collisions at $\sqrt{s}$ = 7 TeV measured with the ATLAS detector at the LHC*, ATLAS-CONF-2011-142.

[5] The ATLAS Collaboration, *Measurement of $t\bar{t}$ production with a veto on additional central jet activity in pp collisions at $\sqrt{s}$ = 7 TeV using the ATLAS detector*, Eur. Phys. J. **C72** (2012), 2043.

[6] The ATLAS Collaboration, *The ATLAS Experiment at the CERN Large Hadron Collider*, JINST **3** (2008), S08003.

[7] L. Evans, (ed.) and P. Bryant, (ed.), *LHC Machine*, JINST **3** (2008), S08001.

[8] The ATLAS Collaboration, *Electron performance measurements with the ATLAS detector using the 2010 LHC proton–proton collision data*, Eur. Phys. J. **C72** (2012), 1909.

[9] W. Lampl et al., *Calorimeter Clustering Algorithms: Description and Performance*, ATL-LARG-PUB-2008-002.

[10] M. Cacciari, G. P. Salam, and G. Soyez, *The Anti-k_t jet clustering algorithm*, JHEP **0804** (2008), 063.

[11] The ATLAS Collaboration, *Jet energy measurement with the ATLAS detector in proton-proton collisions at $\sqrt{s}$ = 7 TeV*, arXiv:1112.6426[hep-ex], (2011).

[12] The ATLAS Collaboration, *Reconstruction and Calibration of Missing Transverse Energy and Performance in Z and W events in ATLAS Proton-Proton Collisions at 7 TeV*, ATLAS-CONF-2011-080.

[13] The ATLAS Collaboration, *Commissioning of the ATLAS high-performance b-tagging algorithms in the 7 TeV collision data*, ATLAS-CONF-2011-102.

[14] The ATLAS Collaboration, *Data-Quality Requirements and Event Cleaning for Jets and Missing Transverse Energy Reconstruction with the ATLAS Detector in Proton-Proton Collisions at a Center-of-Mass Energy of $\sqrt{s}$ = 7 TeV*, ATLAS-CONF-2010-038.

[15] M. L. Mangano et al., *ALPGEN, a generator for hard multiparton processes in hadronic collisions*, JHEP **0307** (2003), 001.

[16] D. Stump et al., *Inclusive jet production, parton distributions, and the search for new physics*, JHEP **0310** (2003), 046.

[17] G. Corcella et al., *HERWIG 6: An Event generator for hadron emission reactions with interfering gluons (including supersymmetric processes)*, JHEP **0101** (2001), 010.

[18] S. Frixione and B. R. Webber, *Matching NLO QCD computations and parton shower simulations*, JHEP **0206** (2002), 029.

[19] S. Alioli, P. Nason, C. Oleari, and E. Re, *A general framework for implementing NLO calculations in shower Monte Carlo programs: the POWHEG BOX*, JHEP **1006** (2010), 043.

[20] H.-L. Lai et al., *New parton distributions for collider physics*, Phys. Rev. **D82** (2010), 074024.

[21] T. Sjöstrand, S. Mrenna, and P. Skands, *PYTHIA 6.4 physics and manual*, JHEP **05** (2006), 026.

[22] The ATLAS Collaboration, *ATLAS tunes of PYTHIA 6 and Pythia 8 for MC11*, ATL-PHYS-PUB-2011-009, 2011.

[23] J. M. Butterworth, J. R. Forshaw, and M. H. Seymour, *Multiparton interactions in photoproduction at HERA*, Z. Phys. **C72** (1996), 637–646.

[24] The ATLAS Collaboration, *First tuning of HERWIG/JIMMY to ATLAS data*, ATL-PHYS-PUB-2010-014, 2010.

[25] H. L. Lai et al., *Global QCD Analysis of Parton Structure of the Nucleon: CTEQ5 Parton Distributions*, Eur. Phys. J. **C12** (2000), 375–392.

[26] P. Z. Skands, *Tuning Monte Carlo Generators: The Perugia Tunes*, Phys. Rev. **D82** (2010), 074018.

[27] B. Cooper, J. Katzy, M. Mangano, A. Messina, L. Mijovic, et al., *Importance of a consistent choice of alpha(s) in the matching of AlpGen and Pythia*, Eur. Phys. J. **C72** (2012), 2078.

[28] M. Aliev et al., *HATHOR - HAdronic Top and Heavy quarks cross section calculatoR"*, Comput. Phys. Commun. **182** (2011), 1034–1046.

[29] B.P. Kersevan and E. Richter-Wąs, *The Monte Carlo event generator AcerMC version 2.0 with interfaces to PYTHIA 6.2 and HERWIG 6.5*, arXiv:0405247[hep-ph], (2004).

[30] N. Kidonakis, *Next-to-next-to-leading-order collinear and soft gluon corrections for t-channel single top quark production*, Phys. Rev. **D83** (2012), 091503.

[31] N. Kidonakis, *NNLL resummation for s-channel single top quark production*, Phys. Rev. **D81** (2010), 054028.

[32] N. Kidonakis, *Two-loop soft anomalous dimensions for single top quark associated production with a W^- or H^-*, Phys. Rev. **D82** (2010), 054018.

[33] S. Agostinelli et al., *Geant4 - A Simulation Toolkit*, Nucl. Instr. and Meth. **A506** (2003), 250.

[34] The ATLAS Collaboration, *The ATLAS Simulation Infrastructure*, Eur. Phys. J. **C70** (2010), 823–874.

[35] The ATLAS Collaboration, *Measurement of the top quark-pair production cross section with ATLAS in pp collisions at $\sqrt{s}$ = 7 TeV*, Eur. Phys. J. **C71** (2011), 1577.

[36] The ATLAS Collaboration, *Top Quark Pair Production Cross-section Measurements in ATLAS in the Single Lepton+Jets Channel without b-tagging*, ATLAS-CONF-2011-023.

[37] The ATLAS Collaboration, *In situ jet pseudorapidity intercalibration of the ATLAS detector using dijet events in $\sqrt{s}$ = 7 TeV proton-proton 2011 data*, ATLAS-CONF-2012-124.

[38] The ATLAS Collaboration, *Light-quark and Gluon Jets: Calorimeter Response, Jet Energy Scale Systematics and Properties*, ATLAS-CONF-2012-138.

[39] The ATLAS Collaboration, *Measurement of the b-tag Efficiency in a Sample of Jets Containing Muons with 5 fb^{-1} of Data from the ATLAS Detector*, ATLAS-CONF-2012-043.

[40] A. Martin, W. Stirling, R. Thorne, and G. Watt, *Parton distributions for the LHC*, Eur. Phys. J. **C63** (2009), 189–285.

[41] The ATLAS Collaboration, *Luminosity Determination in pp Collisions at $\sqrt{s} = 7$ TeV using the ATLAS Detector in 2011*, ATLAS-CONF-2011-116.

[42] G. D'Agostini, *A Multidimensional unfolding method based on Bayes' theorem*, Nucl. Instr. Meth. **A362** (1995), 487–498.

[43] M. L. Mangano, M. Moretti, F. Piccinini, and M. Treccani, *Matching matrix elements and shower evolution for top-quark production in hadronic collisions*, JHEP **0701** (2007), 013.